Infrared and infrared emission spectroscopy of gallium oxide α-GaO(OH) nanostructures

Jing (Jeanne) Yang, Yanyan Zhao and Ray L. Frost •

Inorganic Materials Research Program, School of Physical and Chemical Sciences, Queensland University of Technology, GPO Box 2434, Brisbane Queensland 4001, Australia.

Abstract:

Infrared spectroscopy has been used to study nano to micro sized gallium oxyhydroxide α-GaO(OH), prepared using a low temperature hydrothermal route. Rod-like α-GaO(OH) crystals with average length of ~2.5 μm and width of 1.5 μm were prepared when the initial molar ratio of Ga to OH was 1:3. β-Ga_2O_3 nano and micro-rods were prepared through the calcination of α-GaO(OH) The initial morphology of α-GaO(OH) is retained in the β-Ga_2O_3 nanorods.

The combination of infrared and infrared emission spectroscopy complimented with dynamic thermal analysis were used to characterise the α-GaO(OH) nanotubes and the formation of β-Ga_2O_3 nanorods. Bands at around 2903 and 2836 cm^{-1} are assigned to the -OH stretching vibration of α-GaO(OH) nanorods. Infrared bands at around 952 and 1026 cm^{-1} are assigned to the Ga-OH deformation modes of α-GaO(OH). A significant number of bands are observed in the 620 to 725 cm^{-1} region and are assigned to GaO stretching vibrations.

Keywords: infrared, infrared emission, nanofibres, nanorods, nanomaterials, gallium oxyhydroxide, gallium oxide

• Author to whom correspondence should be addressed (r.frost@qut.edu.au)

Introduction

Synthesis of inorganic nanostructures has been of great interest in material science and nanotechnology in recent times because of wide applications in catalysis, adsorption, ceramics, optical and fluorescence materials, electrochemistry, and so on [1-3]. Gallium oxide (Ga_2O_3), known as gallia, is a ceramic material with high melting point of around 1900 ˚C [4]. Similar to alumina, gallium oxide can crystallize forming the polymorphs α, β, γ, δ and ε-gallia. Ga_2O_3 is normally an insulator at room temperature with a forbidden energy gap of around 4.9 eV and as a semi-conductor above 800 ˚C [5, 6]. Calcination of Ga_2O_3 in a reducing atmosphere turns it into an n-type semiconductor as a result of oxygen vacancies [7]. Ga_2O_3 has been widely used for the preparation of phosphors [8], gas sensor [9, 10] and catalysts [8, 11-13]. Recently, it was also used in the synthesis of solid electrolytes of superior ionic conductivity [14]. Because of the large surface area/volume ratio which is very important for both sensor and catalyst applications, one-dimensional (1D) gallium oxide nanostructures such as nanowires, nanoribbons, nanotubes has been attracted much attention [15-18]. Furthermore, the interesting properties of 1D gallium oxide nanostructure will have great potential for fabricating the next generation of optoelectronic and sensing devices.

Various synthesis methods have been explored to prepare one dimensional gallium oxide nanostructures including the thermal evaporation [19, 20], thermal annealing [21, 22], chemical vapour deposition [23, 24], arc-discharge [25], carbothermal reduction laser ablation[26], oxidation of milling GaN [27], microwave plasma [28], catalyst-assisted methods [29-31]. However, most of these approaches need to be performed at high operation temperature which is around 1300 °C or even above 1600 °C. These methods also involve complex procedures, introducing expensive element as catalyst which may lead to troubles in purification and influence properties of the target materials. Most recently, synthesis 1D nanostructures via soft-chemistry routes at low temperature is attracting great interest due to the obvious advantages, such as, economic, energy efficiency and environmental friendly. Similar to aluminium, gallium oxide hydroxide (GaOOH) is an important precursor for synthesis of gallium oxide Ga_2O_3.

So far limited effort has been devoted to synthesis 1D GaOOH or Ga_2O_3 nanostructures. Sato and Nakamura [32] studied precipitation of GaOOH in solution prepared by mixing gallium

chloride and various alkalis including NaOH, KOH, NH_4OH, $NaHCO_3$ and Na_2CO_3. Hamada et al. [33] reported the formation of monodispersed GaOOH particles with diameter of ~100 nm at the presence of sulphate by hydrolysis at elevated temperatures. Avivi et al. [34] prepared scroll-like cylindrical layered GaOOH crystals with small a mount of metallic Ga enclosed inside via sonochemical reaction. Tas et al. [8] synthesized quadrilateral prisms and spindle-like GaOOH single crystals by forced hydrolysis of Ga^{3+} ions in pure water or in the presence of decomposing urea. The spindles lose their morphology whereas the quadrilateral prisms maintain their morphology after calcination. Cheng and Samulski [35] prepared γ and β-Ga_2O_3 nanotubes by immersing alumina membrane in amorphous $Ga_2O_3 \cdot H_2O$ sol, followed by drying and heating at 500 °C. Patra et al. [36] fabricated submicrometer-sized GaOOH rods by refluxing an aqueous solution of $Ga(NO_3)_3$ and NH_4OH in a microwave oven. Zhang et al. [37] synthesized GaOOH nanorods through a facile large-scale hydrothermal process from $GaCl_3$-H_2O-NaOH solutions under selected pH conditions. Ristić et al. [38] studied application of sol-gel method in the synthesis of gallium oxyhydroxide and gallium oxide by hydrolysis of gallium isopropoxide and $GaCl_3$ in the presence of tetramethylammonium hydroxide in aqueous solution. Most recently, Liu et al. [39] prepared Ga_2O_3 nanorods by the conversion of GaOOH nanorods synthesized via a hydrothermal route using Ga_2O_3 and NaN_3 as precursors. Zhang et al. [40] reported a green hydrothermal method at 200 °C for the synthesis of GaOOH nanorods using Ga_2O_3 and water as starting materials without the presence of surfactant. It is noted that gallium oxide or gallium oxide hydroxide nanostructures synthesised via non-hydrothermal routes are usually thread-like or belt-like which are much longer in length and much smaller in width than that synthesized via hydrothermal routes. To the best of our knowledge, the morphology of Ga_2O_3 or GaOOH reported via hydrothermal approach are generally rod-like or spindle-like crystal with width of ~100 nm which resulted in a small surface area/volume ratio.

The aim of this research is to investigate the influence of experimental procedures on the synthesis and properties of gallium oxide nanomaterials. In this work, we prepared nano to micro sized gallium oxide under different experimental procedures via a soft chemistry route. To make a suitable comparison, nonionic and cationic surfactants were used to obtain more understanding of the growth of gallium oxide. Interestingly, it was observed that Ga_2O_3 nanotubes with width of ~3 nm can be achieved via a low temperature hydrothermal route. To our best knowledge, this is the first report that nanoscaled gallium oxide nanotubes can be

achieved under soft-chemistry synthesis route at a low temperature (100 °C) without any calcination.

Experimental

A $Ga(NO_3)_3$ solution was prepared by dissolving 0.01 mol $Ga(NO_3)_3 \cdot 9H_2O$ into 20 ml ultra-pure water. The pH of the resulting $Ga(NO_3)_3$ solution is in the range of 1.8~1.9. Aqueous 5 M NaOH was added drop-wise to adjust and maintain the pH at fixed value of 7 or 10. Sample was taken as soon as the pH reached the desired value. The resulting fluffy precipitate mixture was then hydrothermally treated at 100˚C for three days or at 180 ˚C for one day. After hydrothermal treatment, all samples were washed by water and dried in air at 80 ˚C. Sample that prepared at pH 7 and treated at 100 ˚C for 3 days is named as S1; Sample that prepared at pH 10 and treated at 100 ˚C for 3 days is named as S2; sample that prepared at pH 10 and treated at 180 ˚C for one day is named as S3. In addition, S1, S2 and S3 were calcined at 900 °C for 2 hours. The heating temperature was raised from room temperature at a rate of 2.5°C/min.

Characterisation

a) A Philips CM 200 transmission electron microscopy (TEM) at 200 KV is used to investigate the morphology of the boehmite nanofibres.
b) Energy-dispersive X-ray (EDX) microanalysis using the TEM was carried out using an Oxford Instruments Link ISIS microanalysis system.
c) XRD analyses were performed on a PANalytical X'Pert PRO X-ray diffractometer, with a Cu X-ray tube (λ = 1.54Å), operating at 45 kV and 35 mA.
d) Raman spectra were collected using an Olympus BHSM microscope, equipped with 10 and 50×objectives and part of a Renishaw 1000 Raman microscope system, which also includes a monochromator, a filter system and a charge coupled device (CCD). Raman spectra were excited by a HeNe laser (532 nm) at a resolution of 2 cm^{-1} in the range between 100 and 4000 cm^{-1}. Repeated acquisition using the highest

magnification was accumulated to improve the signal to noise ratio. Spectra were calibrated using the 520.5 cm^{-1} line of a silicon wafer.

e) FTIR emission spectroscopy was carried out on a Nicolet Nexus 870 FTIR spectrometer equipped with a TGS detector, which was modified by replacing the IR source with an emission cell. A description of the cell and principles of the emission experiment have been published elsewhere [41-44]. Approximately 0.2 mg of boehmite was spread as a thin layer (approximately 0.2 microns) on a 6 mm diameter platinum surface and held in an inert atmosphere within a nitrogen-purged cell during heating.

f) Band component analysis was undertaken using the Jandel 'Peakfit' (Erkrath, Germany) software package which enabled the type of fitting function to be selected and allows specific parameters to be fixed or varied accordingly. Band fitting was done using a Lorentz-Gauss cross-product function with the minimum number of component bands used for the fitting process. The Lorentz-Gauss ratio was maintained at values greater than 0.7 and fitting was undertaken until reproducible results were obtained with squared correlations (r^2) greater than 0.995. Band fitting of the spectra is quite reliable providing there is some band separation or changes in the spectral profile.

Results and Discussion

X-ray diffraction

All the XRD patterns of samples synthesized with and without surfactant are identical. Figure 1 shows the XRD pattern of sample prepared with surfactant PEO. It was noted that GaOOH phase was obtained using low temperature hydrothermal treatment ($\leq 180^{\circ}C$) and Ga_2O_3 generally can be prepared at high temperature ~500 °C as reported in recent studies [8, 34, 36, 37, 39, 40]. All the samples in this study were treated at a relatively low temperature (<100 °C). Interestingly, as shown in Figure 1, the diffraction peaks in the pattern can not be indexed to GaOOH. Although the overall diffraction pattern is broad indicating small particle size in the resulting sample, it can be clearly seen that all the peaks in Figure 1 can be assigned to cubic γ-Ga_2O_3 gallium oxide (JCPDS card No.04-004-4118) rather than monoclinic β-Ga_2O_3 (JCPDS card No. 00-041-1103).

Infrared spectroscopy

The infrared spectra of samples S1, S2 and S3 are shown in Figure 2. A broad H-O-H stretching band at around 3400 cm^{-1} can be observed in spectra of samples synthesized at pH 7 and pH 10 treated at both high temperature and low temperature. It was noted that compared with samples synthesized at pH 10, the H-O-H stretching band position of sample synthesized at pH 7 slightly shifted to higher wavenumbers. No difference in H-O-H stretching band position between samples synthesized at pH 10 but treated at 100 ºC and 180 ºC. A broad peak at around 3480 cm^{-1} was present in the spectra of samples synthesized at pH 7 and pH 10 treated at low temperature but no peak can be observed for sample synthesized at high temperature. The bands at around 2903 and 2836 cm^{-1} can be assigned to the -OH stretching vibration of GaOOH. The spectra also have a broad band at the range of 2298 to 2254 cm^{-1} and a sharp band at ~2030 cm^{-1}. A band at 2038 cm^{-1} and 2020 were also observed in some recent IR studies on α-GaO(OH) rod-like and spindle-like micro sized crystals [26, 45], whereas a band at 2000 cm^{-1} appeared for a mixture of aggregated nanosized α-GaO(OH) particles. The bands at around 1025, 945 and 2030 cm^{-1} are assigned to the Ga-OH bending mode of GaOOH and its overtones, respectively [8, 32] An additional band at around 1630 cm^{-1} can be observed in some of the GaOOH samples and is assigned to the bending mode of H_2O. The presence of band 1359 cm^{-1} was interpreted as symmetric C=O vibration due to specific adsorption of atmospheric CO_2 onto the hydroxide samples during the preparation and processing of FTIR samples in the ambient atmosphere [8]. The group of bands including 690 and 621 cm^{-1} appearing within the range of 1200-600 cm^{-1} is characteristic Ga-O bands seen in hydroxo complexes [46]. It was reported that the band at 690 cm^{-1} is assigned to Ga_2O bending bands [47].

A number of studies of the synthesis and characterisation of GaO(OH) nanomaterials have been reported [48-53]. Previous studies by Huang et al. [50], Ristic et al. [52], and Tas et al. [53] only showed infrared spectra as transmittance spectra and these authors did not undertake any band component analysis to determine precisely how many bands were present in the infrared spectral profile nor did these authors determine the exact position of these bands. Some of the published spectra show the presence of vibrations which can only be

attributed to CH stretching vibrations of organic molecules. In this work, the α-GaO(OH) nanomaterials were synthesised without the use of surfactants or crystal growth directing agents.

Huang noted that as the amount of GaO(OH) increased the spectral profile shifted from ~3400 to 3200 cm^{-1} [50]. This is understandable if the two bands at 2940 and 2850 cm^{-1} increased in intensity. Ristic et al. attributed two bands at 2990 and 3243 cm^{-1} to structural OH units and it is assumed although Ritsic did not state it, the bands are due to GaO(OH) stretching vibrations [52]. The spectra as shown by Tas et al. [53] are poorly resolved and it is not possible to make any valid comparisons. The spectra are further complicated by the presence of urea the presence of which will complicate the spectra through additional NH stretching bands. Liu et al. assigned to broad profile centred at 2850 cm^{-1} to water stretching and GaO(OH) stretching vibrations but did not identify which part of the spectrum was due to these units [51]. These bands were not present in the thermally treated GaO(OH) nanomaterials as the material was converted to either α-Ga_2O_3 or β-Ga_2O_3.

The infrared spectra of the GaO(OH) nanomaterials in the 500 to 1500 cm^{-1} region are shown in Figure 2. In all of the spectra shown in this figure two bands are observed at around 948 and 1017 cm^{-1}. These bands are assigned to the GaOH unit deformation modes. In the spectra shown by Tas et al. [53], two bands are observed at 952 and 1026 cm^{-1} and were assigned to Ga-OH bending modes. These bands were present whether the GaO(OH) nanomaterials was prepared with or without urea [53]. Only when the materials were thermally treated to elevated temperatures were the bands not observed. Obviously the materials had been thermally treated to temperatures above the decomposition temperature of GaO(OH). The reason why two GaOH deformation modes are observed is because there are two different GaOH units in the unit cell of GaO(OH). Huang et al. [50] observed two bands at around 940 and 1020 cm^{-1} for GaO(OH) and assigned the bands to OH bending modes. Ristic et al. showed that the position of these GaOH deformation modes were sensitive to the preparation and subsequent treatment of the GaO(OH) materials [52]. In this work there is some evidence that the GaOH deformation modes are also sensitive to the consequential thermal treatment. The bands are observed at 944 and 1017 cm^{-1} for the GaO(OH) treated at pH=5 at 100°C for 3 days and are found at 948 and 1025 cm^{-1} for GaO(OH) treated at pH=10 at 100°C for 3 days. In comparison the bands are observed at 951 and 1027 cm^{-1} when treated at 180°C at pH=10 for 1 day.

A significant number of bands are observed in the 620 to 725 cm^{-1} region. These bands are assigned to GaO stretching vibrations. For the GaO(OH) treated at pH=5 at 100°C for 3 days infrared bands are observed at 608, 624, 650, 691 and 726 cm^{-1}; for GaO(OH) treated at pH=10 at 100°C for 3 days bands are observed at 621, 639, 658 and 692 cm^{-1}. The number and position of the bands depends upon the thermal treatment and pH of the GaO(OH). There appears to be a band at a position below 525 cm^{-1} which is below the cut-off point of the diamond ATR cell. Ristic et al. found bands at around 500 cm^{-1} [52]. These authors also identified bands at 640 and 688 cm^{-1} with some variation in position depending upon the treatment of the GaO(OH). However no assignment of the bands in these positions was forthcoming. Huang et al. did not record FTIR spectra below ~800 cm^{-1} [50]. Liu assigned bands at 457 and 652 cm^{-1} to Ga_2O bending modes [51]. This assignment appears strange and without foundation. If there is a GaOGa bending vibration then there must first be a GaO stretching vibration. A more likely assignment is the band at 692 cm^{-1} is the GaO stretching vibration and the band at 457 cm^{-1} is the OGaO bending mode. In this research two infrared bands were observed at around 1940 and 2033 cm^{-1}. The assignment of these bands is open to question but one probable attribution is to the first fundamental overtone of the GaO(OH) deformation modes at around 950 and 1017 cm^{-1}. Bands in these positions were observed in the spectra of GaO(OH) by Liu et al. but were not assigned [51]. These authors also found infrared bands at 2343 and 2380 cm^{-1}; these bands are due to atmospheric CO_2 absorption.

The infrared spectra may be compared with the Raman spectra. Raman spectroscopy shows bands characteristic of α-GaO(OH) at 950, ~1000 cm^{-1} attributed to Ga-OH deformation modes. Bands at 261, 275, 433 and 522 cm^{-1} are assigned to vibrational modes involving Ga-OH units. Bands observed at 320, 346, 418 and 472 cm^{-1} are assigned to the deformation modes of Ga_2O_6 octahedra. Two sharp infrared bands at 2948 and 2916 cm^{-1} are attributed to the GaO(OH) symmetric stretching vibrations. Raman spectroscopy of Ga_2O_3 provides bands at 630, 656 and 767 cm^{-1} which are assigned to the bending and stretching of GaO_4 units. Raman bands at 417 and 475 cm^{-1} are attributed to the symmetric stretching modes of GaO_2 units. The Raman bands at 319 and 347 cm^{-1} are assigned to the bending modes of GaO_2 units.

Infrared emission spectroscopy

The infrared emission spectra of α-GaO(OH) are shown in Figures 3, 4 and 5. The significance of these three figures is that different chemical routes are used to synthesise the α-GaO(OH), yet the spectra are identical, as expected.

The infrared emission spectra clearly show a loss of intensity of the bands associated with hydroxyl groups with temperature increase. The intense band at 2950 cm^{-1} is assigned to a combination of water and OH units associated with the α-GaO(OH) structure. No intensity remains in this band at 450 °C. The three bands at 1940, 2050 and 2240 cm^{-1} are assigned to the -OH stretching vibration of α-GaO(OH). The intensity of these bands is also lost by 400°C.

Thermal analysis of α-GaO(OH)

The thermal analysis of α-GaO(OH) is shown in Figure 6. Thermal decomposition of α-GaO(OH) $\rightarrow$ β-Ga_2O_3 occurs at 359 °C. This mass loss is attributed to the dehydroxylation of α-GaO(OH) . A small mass loss at 225 °C also occurs which is attributed to intercalated water.

The reaction is as follows: $2\ \alpha\text{-GaO(OH)} \rightarrow \beta\text{-}Ga_2O_3 + H_2O$

The results of the temperature of the mass loss step is in harmony with the infrared emission results above which showed the loss of OH units by 400 °C.

Conclusions

Infrared emission spectroscopy was used to study the transition of microsized α-GaO(OH) to β-Ga_2O_3 rods. By using soft chemical techniques and low temperatures microsized GaO(OH) nanorods were synthesised. Large crystals were readily obtained. GaO(OH) rod-like micro-sized crystal ~2.5 μm in length and 1.6 μm in width were prepared at 100 ˚C without surfactant via hydrothermal route when the initial Ga to OH ratio was 1:3. The growth of GaO(OH) crystal mainly occurred during ageing and the growth rate dramatically decreased once the nanosized particle aggregate disappeared and the relatively large rod-like crystals were formed. β-Ga_2O_3 crystals were obtained through calcination and the rod-like morphology of the GaO(OH) was retained.

Infrared spectroscopy of α-GaO(OH) enabled bands at 2848 and 2916 $cm^{-1}$are attributed to the α-GaO(OH) symmetric stretching vibrations.

No intensity was observed in these bands after 200°C. Raman bands at 950 and 1010 cm^{-1} are assigned to the hydroxyl deformation modes of α-GaO(OH). After 350 °C the Raman spectrum shows a significantly different pattern to that of α-GaO(OH).. Raman bands are observed at 155, 212, 280, 430, 570 and 685 cm^{-1}. These bands are assigned to β-Ga2O3. Bands at 262, 275, 430, 520 cm^{-1} are assigned to vibrational modes involving Ga-OH units.

Acknowledgements

The financial and infra-structure support of the Queensland University of Technology Inorganic Materials Research Program of the School of Physical and Chemical Sciences is gratefully acknowledged. The Australian Research Council (ARC) is thanked for funding the instrumentation. One of the authors (YZ) is thankful for a Queensland University of

Technology international doctoral scholarship (QIDS) as is one of the authors (JY) for a QUT Inorganic Materials Research Program doctoral scholarship.

References

[1] J.H. Fendler, F.C. Meldrum, Adv. Mat. 7 (1995) 607-632.

[2] S. Iijima, Nature 354 (1991) 56-58.

[3] B.B. Lakshmi, C.J. Patrissi, C.R. Martin, Chem. Mat. 9 (1997) 2544-2550.

[4] S. Gowtham, A. Costales, R. Pandey, Chem. Phys. Lett. 431 (2006) 358-363.

[5] L. Binet, D. Gourier, C. Minot, J. Solid State Chem. 113 (1994) 420-433.

[6] S. Sharma, M.K. Sunkara, J. Am. Chem. Soc. 124 (2002) 12288-12293.

[7] L. Binet, D. Gourier, J. Phys. Chem. Solids 59 (1998) 1241-1249.

[8] A.C. Tas, Peter J. Majewski, F. Aldinger, J. Am. Chem. Soc. 85 (2002) 1421-1429.

[9] M. Ogita, N. Saika, Y. Nakanishi, Y. Hatanaka, Appl.Surf. Sc. 142 (1999) 188-191.

[10] T. Weh, J. Frank, M. Fleischer, H. Meixner, Sens. Actuators B78 (2001) 202-207.

[11] K. Nakagawa, C. Kajita, K. Okumura, N.-o. Ikenaga, M. Nishitani-Gamo, T. Ando, T. Kobayashi, T. Suzuki, J. Catal. 203 (2001) 87-93.

[12] A.L. Petre, A. Auroux, P. Gelin, M. Caldararu, N.I. Ionescu, Thermochim. Act. 379 (2001) 177-185.

[13] B. Xu, B. Zheng, W. Hua, Y. Yue, Z. Gao, J. Catal. 239 (2006) 470-477.

[14] T. Ishihara, H. Matsuda, Y. Takita, J. Am. Chem. Soc. 116 (1994) 3801-3803.

[15] Y. Zhao, R.L. Frost, W.N. Martens, H.Y. Zhu, J. Therm. Anal. Cal. 90 (2007) 755-760.

[16] Y. Zhao, R.L. Frost, W.N. Martens, H.Y. Zhu, Lang. 23 (2007) 9850-9859.

[17] Y. Zhao, R.L. Frost, W.N. Martens, J. Phys. Chem. C111 (2007) 5313-5324.

[18] Y. Zhao, R.L. Frost, J. Yang, W.N. Martens, J. Phys. Chem. C112 (2008) 3568-3579.

[19] L. Dai, L.P. You, X.F. Duan, W.C. Lian, G.G. Qin, J. Cryst. Growth 267 (2004) 538-542.

[20] X. Xiang, C.-B. Cao, Y.-J. Guo, H.-S. Zhu, Chem. Phys. Lett. 378 (2003) 660-664.

[21] W.-S. Jung, H.U. Joo, B.-K. Min, Physica E36 (2007) 226-230.

[22] H.-D. Xiao, H.-L. Ma, C.-S. Xue, H.-Z. Zhuang, J. Ma, F.-J. Zong, X.-J. Zhang, Mat. Chem. Phys. 101 (2007) 99-102.

[23] N.H. Kim, H.W. Kim, C. seoul, C. Lee, Mat. Sc. Eng, B 111 (2004) 131-134.

[24] F. Zhu, Z. Yang, W. Zhou, Y. Zhang, Appl. Surf. Sc. 252 (2006) 7930-7933.

[25] Y.C. Choi, W.S. Kim, Y.S. Park, S.M. Lee, D.J. Bae, Y.H. Lee, G.-S. Park, W.B. Choi, N.S. Lee, J.M. Kim, Adv. Mater. 12 (2000) 746-750.

[26] C.-C. Huang, C.-S. Yeh, C.-J. Ho, J. Phys. Chem. B108 (2004) 4940-4945.
[27] B.C. Kim, K.T. Sun, K.S. Park, K.J. Im, T. Noh, M.Y. Sung, S. Kim, Appl. Phys. Lett. 80 (2002) 481.
[28] F. Zhu, Z.X. Yang, W.M. Zhou, Y.F. Zhang, Solid State Comm. 137 (2006) 177-181.
[29] Y.H. Gao, Y.Bando, T. Sato, Y. F.Zhang, Appl. Phys. Lett. 81 (2002) 2267-2269.
[30] C.H. Liang, G.W. Meng, G.Z. Wang, Y.W. Wang, L.D. Zhang, Appl. Phys. Lett. 78 (2001) 3202-3204.
[31] H.J. Chun, Y.S. Choi, S.Y. Bae, H.W. Seo, S.J. Hong, J. Park, H. Yang, J. Phys. Chem. B107 (2003) 9042-9046.
[32] T. Sato, T. Nakamura, J. Chem. Tech. Biotechnol. 32 (1982) 469-475.
[33] S. Hamada, K. Bando, Y. Kudo, Bull. Chem. Soc. Jpn. 59 (1986) 2063-2069.
[34] S. Avivi, Y. Mastai, G. Hodes, A. Gedanken, J. Am. Chem. Soc. 121 (1999) 4196-4199.
[35] B. Cheng, E.T. Samulski, J. Mater. Chem. 11 (2001) 2901.
[36] C.R. Patra, Y. Mastai, A. Gedanken, J. Nanopart. Res. 6 (2004) 509.
[37] J. Zhang, Z. Liu, C. Lin, J. Lin, J. Crystal Growth 280 (2005) 99-106.
[38] M. Ristic, S. Popovic, S. Music, Mat. Lett. 59 (2005) 1227-1233.
[39] X. Liu, G. Qiu, Y. Zhao, N. Zhang, R. Yi, J. Alloy. Comp. 439 (2007) 275-278.
[40] Y.C. Zhang, X. Wu, X.Y. Hu, Q.F. Shi, Materials Letters 61 (2007) 1497-1499.
[41] R.L. Frost, A.M. Vassallo, Clays Clay Miner. 44 (1996) 635-651.
[42] R.L. Frost, A.M. Vassallo, Mikrochim. Acta, Suppl. 14 (1997) 789-791.
[43] R.L. Frost, J.T. Kloprogge, Spectrochim. Acta, 55A (1999) 2195-2205.
[44] R.L. Frost, M.L. Weier, Thermochim. Act. 406 (2003) 221-232.
[45] X. Liu, G. Qiu, Y. Zhao, N. Zhang, R. Yi, J. Alloys Comp. 439 (2007) 275-278.
[46] G. Socrates, Infrared Characteristic Group Frequencies, Wiley, New York, 1994.
[47] A.J. Hinchclife, J.S. Ogden, J. Phys. Chem. (1973) 2537.
[48] S. Avivi, Y. Mastai, G. Hodes, A. Gedanken, J. Am. Chem. Soc. 121 (1999) 4196-4199.
[49] B.J. Clapsaddle, D.W. Sprehn, A.E. Gash, J.H. Satcher, Jr., R.L. Simpson, J. Non-Cryst. Solids 350 (2004) 173-181.
[50] C.-C. Huang, C.-S. Yeh, C.-J. Ho, J. Phys. Chem. B108 (2004) 4940-4945.
[51] X. Liu, G. Qiu, Y. Zhao, N. Zhang, R. Yi, J. Alloys Comp. 439 (2007) 275-278.
[52] M. Ristic, S. Popovic, S. Music, Mat. Lett. 59 (2005) 1227-1233.

[53] A.C. Tas, P.J. Majewski, F. Aldinger, J. Am. Ceram. Soc. 85 (2002) 1421-1429.

397

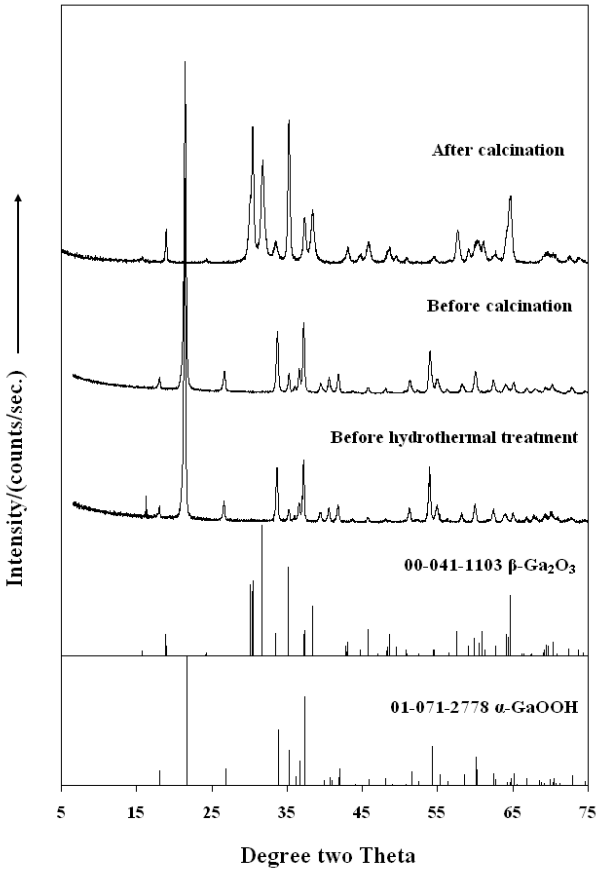

398

399

400 **Figure 1 XRD patterns for samples synthesized**

401

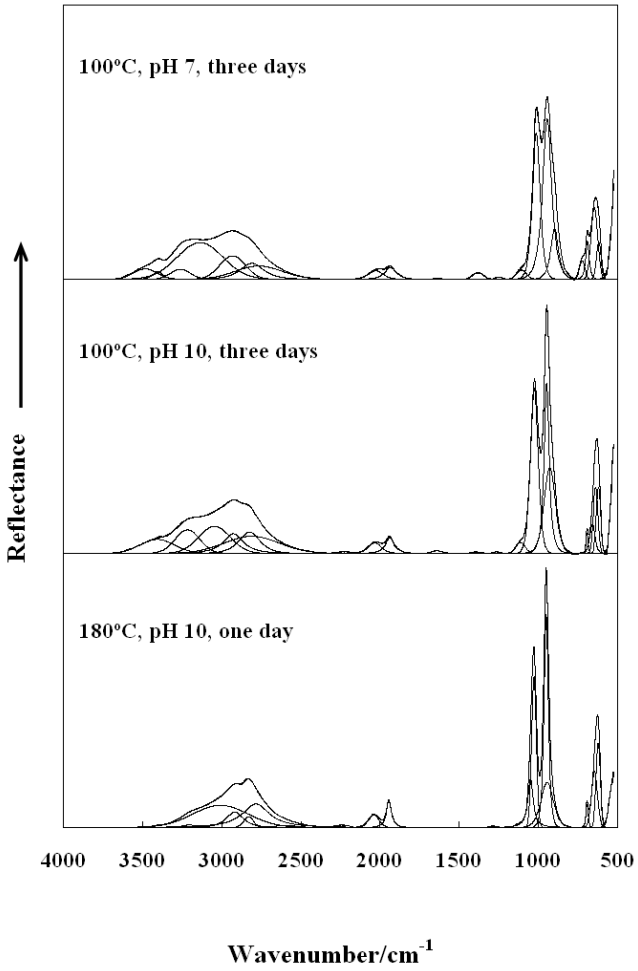

402

403

404 **Figure 2**

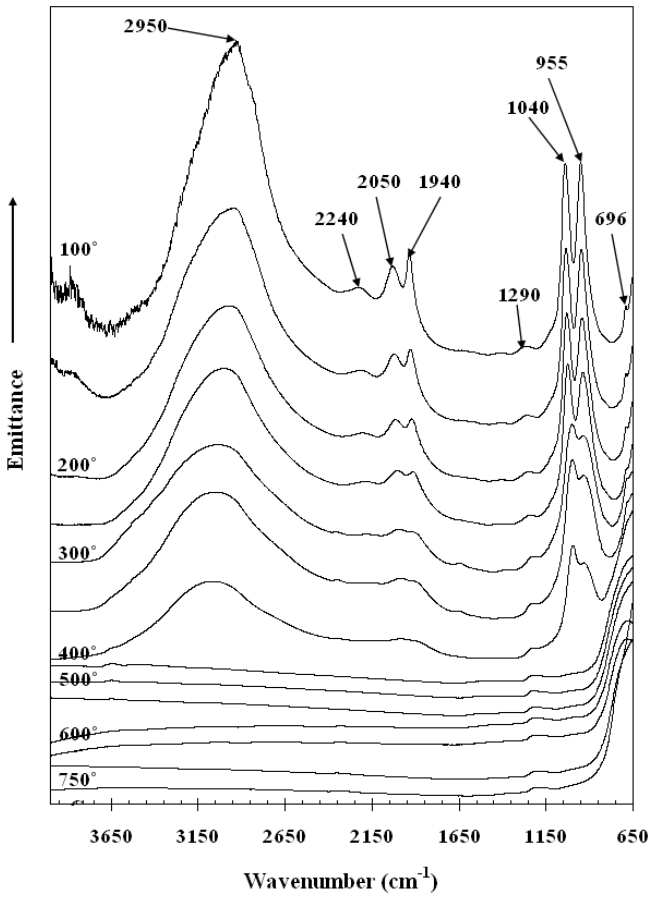

405

406

407 **Figure 3 2D3**

408

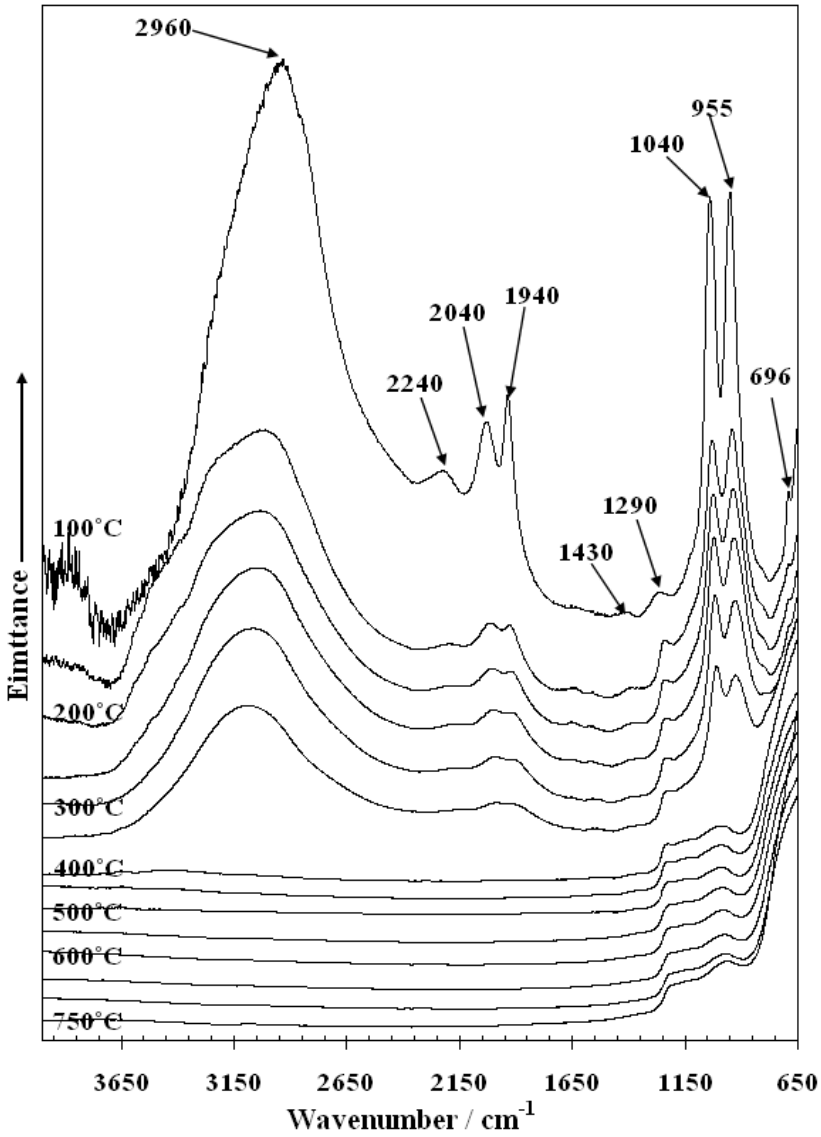

409

410

411

412 **Figure 4 F34**

413

414

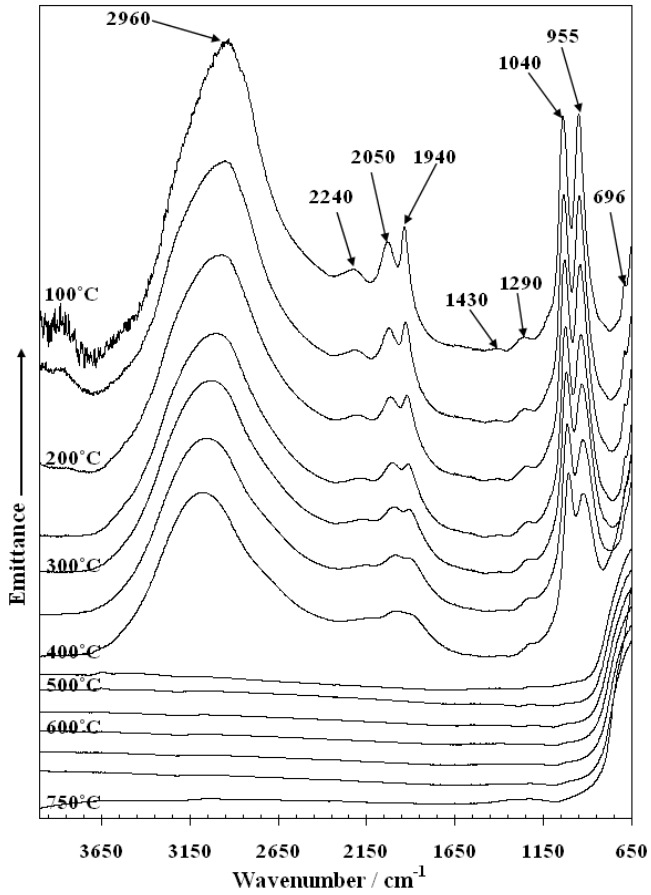
2960
955
1040
2050
1940
2240
696
1290
1430
100°C
200°C
300°C
400°C
500°C
600°C
750°C
Emittance
3650
3150
2650
2150
1650
1150
650
Wavenumber / cm-1

Figure 5 F32

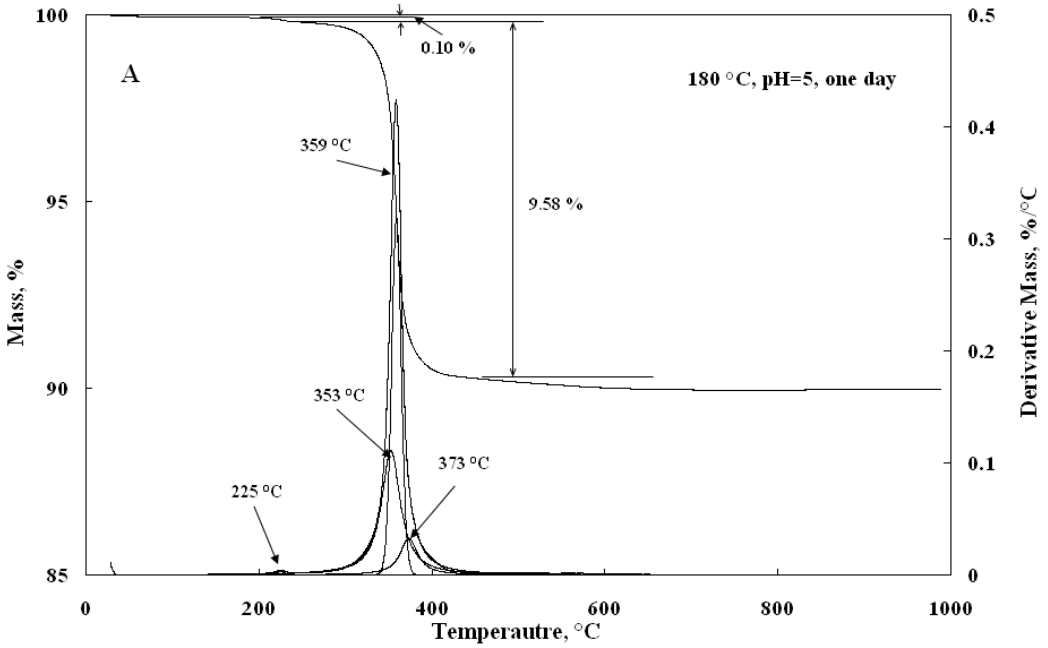

Figure 6 Thermal analysis of GaO(OH)